IOPscience iopscience.iop.org

Home Search Collections Journals About Contact us My IOPscience

# Application of Haar wavelets to time-domain BEM for the transient scalar wave equation

This content has been downloaded from IOPscience. Please scroll down to see the full text.

2010 IOP Conf. Ser.: Mater. Sci. Eng. 10 012222

(http://iopscience.iop.org/1757-899X/10/1/012222)

View the table of contents for this issue, or go to the journal homepage for more

Download details:

IP Address: 133.35.104.141
This content was downloaded on 23/10/2013 at 06:17

Please note that terms and conditions apply.

IOP Conf. Series: Materials Science and Engineering **10** (2010) 012222 doi:10.1088/1757-899X/10/1/012222

# Application of Haar wavelets to time-domain BEM for the transient scalar wave equation

**Kazuhiro Koro**[1], **Kazuhisa Abe**[2]

[1] Associate Professor, Department of Civil Engineering & Architecture, Niigata University, 8050 Igarashi 2-Nocho, Nishi-ku, Niigata, 950-2181, Japan

[2] Professor, Department of Civil Engineering & Architecture, Niigata University, 8050 Igarashi 2-Nocho, Nishi-ku, Niigata, 950-2181, Japan

E-mail: kouro@eng.niigata-u.ac.jp

**Abstract.** The time-domain boundary element method using the Haar wavelets is developed for reducing the computational cost of the BE wave propagation analysis. The Haar wavelets are used for the discretization of the boundary integral equation. The time variation of the unknown potential and flux is approximated using the conventional scheme. The small matrix entries of the coefficient matrix are truncated with the Beylkin-type matrix compression scheme at before and after calculation of double boundary integral. The present BEM has the numerical stability comparable to the piecewise constant Galerkin BEM. The sparsity of the coefficient matrix generated at an each time step rises as the time step proceeds; the memory requirement of the present method can be reduced in comparison with the conventional BEM. The reduction of the computational work from the conventional BE analysis is difficult because of the sparse system of the conventional time-domain BEM.

## 1. Introduction

Nowadays, the fast solutions for the boundary element method (BEM), e.g. the fast multipole expansion method [1] and the wavelet method (wavelet BEM) [2-4], have been developed for reducing the computational work and the memory requirements. In the wavelet method, the wavelets have the following two roles: (i) the basis functions for approximating the unknowns of the boundary integral equation, and (ii) the weighting functions for the Galerkin discretization. The coefficient matrices generated by the wavelet method have small matrix entries due to the vanishing moment property of the wavelets. The truncation of the small matrix entries enables us to replace the dense system for the conventional BEM into the sparse one. The sparse system of the discretized equation corresponding to the boundary integral equation leads to the reduction of the computational work and the memory requirements [5-16]. The similar sparse matrix can be generated also by applying the fast wavelet transform (FWT) to the coefficient matrix and truncating the resulting small matrix entries [5-12].

Many researchers on the wavelet BEM have discussed on the performance in Laplace problems and Helmholtz problems. For the BE analysis of these problems, a sparse coeffient matrix enables us to not only memory reduction but also the reduction of the $O(N^3)$ computational work for solving the discretized equations. Ravnik et al have applied the wavelet BEM to the incompressible viscous flow problems [9-12]; the wavelet method is used for the BE analysis of the Poisson's equation in the vorticity-velocity formulation. The BEM is however, applied to the unsteady state problems e.g. the unsteady heat transfer problems, the diffusion problems and the wave propagation problems [13]. For wave propagation problems, the BE solutions satisfy the Sommerfelt radiation condition, which is a main advantage of the

© 2010 Published under licence by IOP Publishing Ltd 

BEM. The unsteady BE analysis of the wave equation is based on either the following two formulations: (i) the superposion of the frequency-domain solutions using the fast Fourier transform (FFT), and (ii) the discretization of the time-domain boundary integral equation [13]. The time-domain BE formulation, in particular, enables us easily to deal with the nonlinearity in a part of domain or boundary using e.g. the BE-FE coupling methods. In the time-domain BE analysis, the time convolution is calculated by the matrix-vector multiplication of the order $O(MN^2)$ ($N$: the degree of freedom (DOF)) at an arbitrary time step $M$. The discretized time convolution thus needs to large computational work and memory requirements. Soares et al [14, 15] have attempted the computational cost reduction of time convolution in the time-domain BEM. The wavelet method is effective also for the reduction of this computational cost. Ravnik et al [9] have used the wavelet method for reducing the computational cost for the incompressible viscous flow simulation using the time-dependent fundamental solutions. Koro et al [16] have investigated on the performance of the time-domain wavelet BEM for the diffusion problems. However, the application of the wavelet method to the time-domain BE wave propagation analysis has never been attempted.

In the present paper, we develop the time-domain BEM using the Haar wavelets for 2-D scalar wave equation. The Haar wavelets will be used as the basis functions of the approximations of the potential and the flux on the boundary and the weighting functions for the Galerkin discretization. The resulting algebraic equations have the sparse coefficient matrices generated by the truncation of the small matrix entries. The validity of our formulation, the numerical stability and the computational performance of the present method will be investigated through numerical results.

## 2. Time-domain boundary integral equation

Let us consider two-dimensional transient scalar wave propagation problems. The governing wave equation, the boundary conditions and the initial conditions are expressed as follows:

$$\nabla^2 u(\boldsymbol{x},t) - \frac{1}{c^2}\ddot{u}(\boldsymbol{x},t) = 0, \qquad (\text{in } \Omega) \tag{1}$$

$$u = \bar{u}\ (\text{on } \Gamma_u), \qquad q = \frac{\partial u}{\partial n} = \bar{q}, \qquad (\text{on } \Gamma_q) \tag{2}$$

$$u(\boldsymbol{x},0) = u_0(\boldsymbol{x}), \qquad \dot{u}(\boldsymbol{x},0) = v_0(\boldsymbol{x}), \qquad (\text{in } \Omega) \tag{3}$$

where $\boldsymbol{x}$ is a material point, $\nabla$ is the nabla operator, $t$ is time and $\dot{}$ denotes the time derivative. $\Omega$ is the domain, $\Gamma$ is the boundary, and has the sub-boundary $\Gamma_u$, $\Gamma_q$ with $\Gamma_u \cup \Gamma_q = \Gamma$ and $\Gamma_u \cap \Gamma_q = \emptyset$. $u$ is the potential, $q$ is the flux and $c$ is the wave speed. $n$ is the outward normal at a point $\boldsymbol{x}$ on the boundary $\Gamma$. $\bar{u}$ and $\bar{q}$ in the boundary conditions (2) and $u_0$ and $v_0$ in the initial conditions (3) are the known scalar functions.

The time-domain boundary integral equation corresponding to the initial and the boundary value problem (1)-(3) is given by

$$\begin{aligned}\alpha(\boldsymbol{y})u(\boldsymbol{y},\tau) = &\int_0^\tau \int_\Gamma \Big[u^*(\boldsymbol{x},t;\boldsymbol{y},\tau)q(\boldsymbol{x},t) - q^*(\boldsymbol{x},t;\boldsymbol{y},\tau)u(\boldsymbol{x},t)\Big]\, d\Gamma_x dt \\ &+ \frac{1}{c^2}\int_\Omega \Big[u^*(\boldsymbol{x},0;\boldsymbol{y},\tau)v_0(\boldsymbol{x}) - \dot{u}^*(\boldsymbol{x},0;\boldsymbol{y},\tau)u_0(\boldsymbol{x})\Big]\, d\Omega_x,\end{aligned} \tag{4}$$

where $\boldsymbol{y} \in \Gamma$, and the free term $\alpha(\boldsymbol{y})$ is $1/2$ at a point on a smooth boundary. The fundamental solutions for 2-D scalar wave problems, $u^*$ and $q^*$, have the following forms:

$$\begin{aligned}u^*(\boldsymbol{x},t;\boldsymbol{y},\tau) &:= \frac{c}{2\pi}\frac{H(c(\tau-t)-r)}{\sqrt{c^2(\tau-t)^2 - r^2}}, \\ q^*(\boldsymbol{x},t;\boldsymbol{y},\tau) &:= \frac{\partial u^*}{\partial n} = \frac{c}{2\pi}\frac{\partial r}{\partial n}\left[\frac{rH(c(\tau-t)-r)}{\{c^2(\tau-t)^2 - r^2\}^{3/2}} - \frac{\delta(c(\tau-t)-r)}{\sqrt{c^2(\tau-t)^2 - r^2}}\right],\end{aligned} \tag{5}$$

where $r = |\boldsymbol{x} - \boldsymbol{y}|$, $H(\cdot)$ is Heaviside's step function and $\delta(\cdot)$ is Dirac's delta function.

We now apply the regularization proposed by Mansur & Brebbia [13] to the integral equation (4). For the initial condition $u(\boldsymbol{x}, 0) = u_0(\boldsymbol{x}) = 0$ and $\dot{u}(\boldsymbol{x}, 0) = v(\boldsymbol{x}) = 0$, the time-domain regularized boundary intagral equation has the form

$$\begin{aligned}\alpha(\boldsymbol{y})u(\boldsymbol{y},\tau) = &\int_\Gamma \int_0^\tau u^*(\boldsymbol{x},t;\boldsymbol{y},\tau)q(\boldsymbol{x},t)dtd\Gamma_x \\ &+ \int_\Gamma \int_0^\tau \left[q_1^*(\boldsymbol{x},t;\boldsymbol{y},\tau)u(\boldsymbol{x},t) + q_2^*(\boldsymbol{x},t;\boldsymbol{y},\tau)\dot{u}(\boldsymbol{x},t)\right] dtd\Gamma_x,\end{aligned} \tag{6}$$

where $q_0^*$, $q_1^*$ and $q_2^*$ are defined by

$$\begin{aligned}q_0^*(\boldsymbol{x};\boldsymbol{y},\tau) &:= \frac{r}{2\pi c^2}\frac{\partial r}{\partial n}\frac{H(c(\tau-t)-r)}{\tau\sqrt{\tau^2-(r/c)^2}}, \\ q_1^*(\boldsymbol{x},t;\boldsymbol{y},\tau) &:= \frac{r}{2\pi c^2}\frac{\partial r}{\partial n}\frac{H(c(\tau-t)-r)}{(\tau-t)^2\sqrt{(\tau-t)^2-(r/c)^2}}, \\ q_2^*(\boldsymbol{x},t;\boldsymbol{y},\tau) &:= (\tau-t)\cdot q_1^*(\boldsymbol{x},t;\boldsymbol{y},\tau).\end{aligned} \tag{7}$$

In the present paper, we discuss the computational cost reduction of the boundary element analysis based on the equation (6). Note that our formulation using Mansur's regularization [13] is *not essential* for applying the wavelet method to the time-domain BEM for the 2-D wave equation.

## 3. Discretization of time-domain boundary integral equation using Haar wavelets

To derive the discretized algebraic equations from the time-domain boundary integral equation (6), we first require to approximate the unknown boundary values $u$ and $q$ in time and space.

The approximation in time domain are constructed by the conventional scheme. We now assume to satisfy Eq.(6) at the time $\tau = t_L = L\Delta t$. The time integration in Eq.(6) which is then defined on the intelval [0, $t_L$] is divided into the $L$ subintervals [$t_{p-1}$, $t_p$] ($t_p = p\Delta t$, $\Delta t$: time step width, $p = 1, 2, \ldots, L$). The unknowns $u(\boldsymbol{x}, t)$, $q(\boldsymbol{x}, t)$ and $\dot{u}(\boldsymbol{x}, t)$ in a subinterval [$t_{p-1}$, $t_p$] are approximated by

$$\begin{aligned}u(\boldsymbol{x},t) &\approx \frac{t_p - t}{\Delta t}u(\boldsymbol{x},t_{p-1}) + \frac{t - t_{p-1}}{\Delta t}u(\boldsymbol{x},t_p) = \frac{t_p - t}{\Delta t}u(\boldsymbol{x})^{(p-1)} + \frac{t - t_{p-1}}{\Delta t}u(\boldsymbol{x})^{(p)}, \\ q(\boldsymbol{x},t) &\approx q(\boldsymbol{x},t_p) = q(\boldsymbol{x})^{(p)}, \qquad \dot{u}(\boldsymbol{x},t) \approx \frac{u(\boldsymbol{x})^{(p)} - u(\boldsymbol{x})^{(p-1)}}{\Delta t}.\end{aligned} \tag{8}$$

In other words, the approximation in time domain consists of the linear interpolation of $u$, the backward piecewise constant interpolation of $q$ and the backward difference of $\dot{u}$.

Substituting Eq.(8) into Eq.(6), we now obtain the boundary integral equation as follows:

$$\begin{aligned}&\alpha(\boldsymbol{y})u^{(L)}(\boldsymbol{y}) - \int_\Gamma Q_{1,L}^{*(L)}(\boldsymbol{x};\boldsymbol{y})u^{(L)}(\boldsymbol{x})d\Gamma_x - \int_\Gamma U_L^{*(L)}(\boldsymbol{x};\boldsymbol{y})q^{(L)}(\boldsymbol{x})d\Gamma_x \\ &= \sum_{p=1}^{L-1}\int_\Gamma \left[U_p^{*(L)}(\boldsymbol{x};\boldsymbol{y})q^{(p)}(\boldsymbol{x}) + Q_{1,p}^{*(L)}(\boldsymbol{x};\boldsymbol{y})u^{(p)}(\boldsymbol{x})\right]d\Gamma_x + \sum_{p=1}^{L}\int_\Gamma Q_{2,p}^{*(L)}(\boldsymbol{x};\boldsymbol{y})u^{(p-1)}(\boldsymbol{x})d\Gamma_x,\end{aligned} \tag{9}$$

where $u^{(L)}(\boldsymbol{y}) = u(\boldsymbol{y}, t_L)$ and $q^{(L)}(\boldsymbol{y}) = q(\boldsymbol{y}, t_L)$. The fundamental solutions $U_p^{*(L)}$, $Q_{1,p}^{*(L)}$ and $Q_{2,p}^{*(L)}$

are defined as

$$
\begin{aligned}
U_p^{*(L)}(\boldsymbol{x};\boldsymbol{y}) &:= \frac{1}{2\pi}\int_{t_{p-1}}^{t_p} \frac{H(c(t_L-t)-r)}{\sqrt{(t_L-t)^2-(r/c)^2}}dt,\\
Q_{1,p}^{*(L)}(\boldsymbol{x};\boldsymbol{y}) &:= \frac{(L-p+1)r}{2\pi c^2}\frac{\partial r}{\partial n}\int_{t_{p-1}}^{t_p} \frac{H(c(t_L-t)-r)}{(t_L-t)^2\sqrt{(t_L-t)^2-(r/c)^2}}dt,\\
Q_{2,p}^{*(L)}(\boldsymbol{x};\boldsymbol{y}) &:= \frac{(p-L)r}{2\pi c^2}\frac{\partial r}{\partial n}\int_{t_{p-1}}^{t_p} \frac{H(c(t_L-t)-r)}{(t_L-t)^2\sqrt{(t_L-t)^2-(r/c)^2}}dt.
\end{aligned}
\tag{10}
$$

We next show the derivation of the discretized algebraic equations from the boundary integral equation (9). The potential $u^{(p)}$ and the flux $q^{(p)}$ at $t = t_L$ are approximated by the wavelet series using the Haar wavelets [3] as

$$
\begin{aligned}
u^{(p)}(\boldsymbol{x}) \approx \tilde{u}^{(p)}(\boldsymbol{x}) &= \sum_{i=1}^{N} U_i^{(p)} w_i(\boldsymbol{x}) := \sum_{j=1}^{n_s} \hat{u}_j^{(p)}\phi_{0,j}(\boldsymbol{x}) + \sum_{k=0}^{m_r}\sum_{l=1}^{n_w(k)} \tilde{u}_{k,l}^{(p)}\psi_{k,l}(\boldsymbol{x}),\\
q^{(p)}(\boldsymbol{x}) \approx \tilde{q}^{(p)}(\boldsymbol{x}) &= \sum_{i=1}^{N} Q_i^{(p)} w_i(\boldsymbol{x}) := \sum_{j=1}^{n_s} \hat{q}_j^{(p)}\phi_{0,j}(\boldsymbol{x}) + \sum_{k=0}^{m_r}\sum_{l=1}^{n_w(k)} \tilde{q}_{k,l}^{(p)}\psi_{k,l}(\boldsymbol{x}),
\end{aligned}
\tag{11}
$$

where $p = 0, 1, \ldots$. $\phi_{0,j}$ is the scaling function defined as the piecewise constant function, and $\psi_{k,l}$ is the Haar wavelet. $\hat{u}_j^{(p)}$, $\tilde{u}_{k,l}^{(p)}$, $\hat{q}_j^{(p)}$ and $\tilde{q}_{k,l}^{(p)}$ are wavelet expansion coefficients. The basis $w_i(\boldsymbol{x})$ is given by either $\phi_j$ or $\psi_{k,l}$. $N$ is the degree of freedom (DOF).

Substituting Eq.(11) into Eq.(9), we obtain the residual $r(\boldsymbol{y})$ as

$$
\begin{aligned}
r(\boldsymbol{y}) := \alpha(\boldsymbol{y})\tilde{u}^{(L)}(\boldsymbol{y}) &- \int_\Gamma U_L^{*(L)}(\boldsymbol{x};\boldsymbol{y})\tilde{q}^{(L)}(\boldsymbol{x})d\Gamma_x - \int_\Gamma Q_{1,L}^{*(L)}(\boldsymbol{x};\boldsymbol{y})\tilde{u}^{(L)}(\boldsymbol{x})d\Gamma_x\\
- \sum_{p=1}^{L-1}\int_\Gamma \left[U_p^{*(L)}(\boldsymbol{x};\boldsymbol{y})\tilde{q}^{(p)}(\boldsymbol{x}) + Q_{1,p}^{*(L)}(\boldsymbol{x};\boldsymbol{y})\tilde{u}^{(p)}(\boldsymbol{x})\right]d\Gamma_x &- \sum_{p=1}^{L}\int_\Gamma Q_{2,p}^{*(L)}(\boldsymbol{x};\boldsymbol{y})\tilde{u}^{(p-1)}(\boldsymbol{x})d\Gamma_x.
\end{aligned}
\tag{12}
$$

The residual (12) is required to satisfy the following Galerkin conditions:

$$
\int_\Gamma r(\boldsymbol{y})w_i(\boldsymbol{y})d\Gamma_y = 0, \qquad (i = 1, 2, \ldots, N)
\tag{13}
$$

As a result, the following linear algebraic equations are obtained as

$$
\boldsymbol{H}_{1,L}^{(L)}\boldsymbol{u}^{(L)} - \boldsymbol{G}_L^{(L)}\boldsymbol{q}^{(L)} = \sum_{p=1}^{L-1}\boldsymbol{G}_p^{(L)}\boldsymbol{q}^{(p)} - \sum_{p=1}^{L-1}\boldsymbol{H}_{1,p}^{(L)}\boldsymbol{u}^{(p)} + \sum_{p=1}^{L}\boldsymbol{H}_{2,p}^{(L)}\boldsymbol{u}^{(p-1)},
\tag{14}
$$

where the vectors $\boldsymbol{u}^{(p)}$ and $\boldsymbol{q}^{(p)}$ consist of the expansion coefficients $U_i^{(p)}$ and $Q_i^{(p)}$ $(i = 1, 2, \ldots, N)$, respectively. The coefficient matrices $\boldsymbol{G}_p^{(L)}$, $\boldsymbol{H}_{1,p}^{(L)}$ and $\boldsymbol{H}_{2,p}^{(L)}$ have matrix entries $g_{p,ij}^{(L)}$, $h_{1,p,ij}^{(L)}$ and $h_{2,p,ij}^{(L)}$ as:

$$
\begin{aligned}
g_{p,ij}^{(L)} &:= \int_\Gamma w_i(\boldsymbol{y})\int_\Gamma U_p^{*(L)}(\boldsymbol{x};\boldsymbol{y})w_j(\boldsymbol{x})d\Gamma_x d\Gamma_y,\\
h_{1,p,ij}^{(L)} &:= \delta_{Lp}\int_\Gamma \alpha(\boldsymbol{y})w_i(\boldsymbol{y})w_j(\boldsymbol{y})d\Gamma_y - \int_\Gamma w_i(\boldsymbol{y})\int_\Gamma Q_{1,p}^{*(L)}(\boldsymbol{x};\boldsymbol{y})w_j(\boldsymbol{x})d\Gamma_x d\Gamma_y,\\
h_{2,p,ij}^{(L)} &:= \int_\Gamma w_i(\boldsymbol{y})\int_\Gamma Q_{2,p}^{*(L)}(\boldsymbol{x};\boldsymbol{y})w_j(\boldsymbol{x})d\Gamma_x d\Gamma_y.
\end{aligned}
\tag{15}
$$

## 4. Matrix compression scheme

In the wavelet BEM, the sparse coefficient matrices in Eq.(14) can be generated by *truncation* (regarding the small matrix entries as null entries), which leads to the reduction of the memory requirement and the computational work. The truncated entries of the coefficient matrices $\boldsymbol{G}_p^{(L)}$, $\boldsymbol{H}_{1,p}^{(L)}$ and $\boldsymbol{H}_{2,p}^{(L)}$ ($p = 1, 2, \ldots, L$) are selected using the elements $g_{p,ij}^{(L)}$ of the matrix $\boldsymbol{G}_p^{(L)}$.

At the stage before calculation of the element (15), *a priori* truncation is carried out using the following Beylkin-type criterion:

$$\bar{g}_{p,ij}^{(L)} < \kappa \cdot g_{ref}, \tag{16}$$

where $\kappa$ is the threshold of the truncation, and $g_{ref}$ is the representative value of $|g_{p,ij}^{(L)}|$. $\bar{g}_{p,ij}^{(L)}$ is the approximation of $|g_{p,ij}^{(L)}|$. This selection of the truncated entries enables us to reduce the computational work on the generation of the truncated matrix entries.

After the calculation of Eq.(15), we select the truncated entries again as *a posteriori* truncation. The criterion of the second truncation is defined by

$$|g_{p,ij}^{(L)}| < \kappa \cdot g_{ref}. \tag{17}$$

We now derive the concrete form of the approximation $\bar{g}_{p,ij}^{(L)}$ in Eq.(16). To calculate the boundary integrals included in $g_{p,ij}^{(L)}$ of Eq.(15), we first introduce the intrinsic coordinates $-1 \leq \xi \leq 1$ and $-1 \leq \eta \leq 1$. Substituting $d\Gamma_y = J_i(\xi)d\xi$, $d\Gamma_x = J_j(\eta)d\eta$, $J_i(\xi) \approx J_i(\xi = 0) := \bar{J}_i$ and $J_j(\eta) \approx J_j(\eta = 0) := \bar{J}_j$ into Eq.(15), we have

$$g_{p,ij}^{(L)} \approx \bar{J}_i \bar{J}_j \int_{-1}^{1} w_i(\xi) \int_{-1}^{1} U_p^{*(L)}(\xi, \eta) w_j(\eta) d\eta d\xi, \tag{18}$$

where the basis functions $w_i$ and $w_j$ have the $n_i$th and the $n_j$th vanishing moments, respectively. The absolute value of the matrix element $g_{p,ij}^{(L)}$ can be approximated by

$$|g_{p,ij}^{(L)}| \approx \frac{\bar{J}_i \bar{J}_j}{n_i! n_j!} \left| \left( \frac{\partial r}{\partial \xi} \right)^{n_i} \right|_{\xi=0} \cdot \left| \left( \frac{\partial r}{\partial \eta} \right)^{n_j} \right|_{\eta=0} \cdot \left| \frac{\partial^{n_i+n_j} U_p^{*(L)}}{\partial r^{n_i+n_j}} \right|_{\xi=\eta=0} \cdot \left| \int_{-1}^{1} \xi^{n_i} w_i(\xi) d\xi \right| \cdot \left| \int_{-1}^{1} \eta^{n_j} w_j(\eta) d\eta \right|. \tag{19}$$

In consideration of the definition and the approximation as

$$\beta_i := \int_{-1}^{1} \xi^{n_i} w_i(\xi) d\xi, \quad \beta_j := \int_{-1}^{1} \eta^{n_j} w_j(\eta) d\eta, \quad \left| \left( \frac{\partial r}{\partial \xi} \right)^{n_i} \right|_{\xi=0} \approx \bar{J}_i^{n_i}, \quad \left| \left( \frac{\partial r}{\partial \eta} \right)^{n_j} \right|_{\eta=0} \approx \bar{J}_j^{n_j}, \tag{20}$$

we have the following approximation $\bar{g}_{p,ij}^{(L)}$ of the absolute value $|g_{p,ij}^{(L)}|$:

$$|g_{p,ij}^{(L)}| \approx \bar{g}_{p,ij}^{(L)} := \frac{|\beta_i||\beta_j| \bar{J}_i^{1+n_i} \bar{J}_j^{1+n_j}}{n_i! n_j!} \cdot \left| \frac{\partial^{n_i+n_j} U_p^{*(L)}}{\partial r^{n_i+n_j}} \right|_{\xi=\eta=0}. \tag{21}$$

## 5. Numerical Results

The test example for investigating the numerical stability and the computational cost of the present wavelet BEM is shown in figure 1 with the initial conditions $u_0 = 0$ and $v_0 = 0$. The wave speed is $c = 1$. The exact solution of this example is expressed as

$$\begin{aligned} u(x,t) = {} & H(ct - x) \cdot (ct - x) - H(ct + x - 4) \cdot (ct + x - 4) \\ & - H(ct - 4 - x) \cdot (ct - 4 - x) + H(ct + x - 8) \cdot (ct + x - 8), \end{aligned} \tag{22}$$

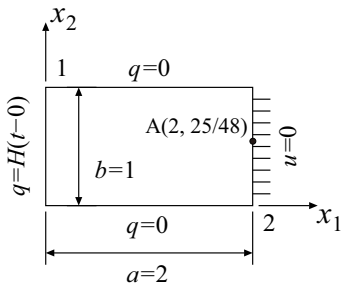


**Figure 1.** Test problem.

where $0 \leq t \leq T$ ($T = 8/c$), and has the periodicity with period $T$ as

$$u(x, t + kT) = u(x, t), \qquad (k : \text{integer}). \tag{23}$$

In the BE simulation, we use the Haar wavelet with 18 scaling functions. The iterative solver is the GMRES method with the Jacobi preconditiong.

### *5.1. Numerical stability*

We first investigate the numerical stability of the present wavelet BEM. In the BE analysis for the test example, the time domain is prescribed as $0 \leq t \leq 2T$. The approximation for $u$ and $q$ are constructed with 18 scaling functions and $m_r = 2$. The DOF is $N = 18 \cdot 2^{m_r+1} = 144$. The truncation for matrix compression is *not* carried out. The time step width is set to $\Delta t = \beta \ell_{ref}/c$ ($\beta = 0.3$, 0.5, 0.7, 1.0, $\ell_{ref} = 1/24$). The error $e(t)$ of the potential $u$ is defined as

$$e(t) := \sum_{i=1}^{N} \left| \tilde{u}(\boldsymbol{x}_i, t) - u_{true}(\boldsymbol{x}_i, t) \right| \ell_i, \tag{24}$$

where $\tilde{u}$ is the BE solution, $u_{true}$ is the exact solution at the point $\boldsymbol{x}_i$, and $\ell_i$ is the support width in which the BE solution shows a piecewise constant value.

Figure 2 shows the time history of the error $e(t)$. Figure 3 depicts the flux $q$ at the point A $(2, 25/48)$. In the conventional BEM, the piecewise constant collocation BEM has the numerical instability on the time step width; for the smaller values of $\beta$ (e.g. $\beta \leq 0.5$) the error of the BE solution increases with the progress of the time marching. The time step width corresponding to a larger value of $\beta$ may contribute to stabilize the time-domain collocation BEM. The Galerkin discretization enables us to implement the BE analysis without the above numerical instability, as pointed out in Ref.[17].

The present wavelet BEM tends to be more stable than the piecewise constant collocation BEM, as shown in figure 2 and figure 3. The slight high frequency noises are observed in the time history of the flux $q$; the numerical stability of the present wavelet BEM is comparable to the conventional Galerkin BEM.

### *5.2. Reduction of memory requirements*

We next investigate the reduction of the memory requirements. In the numerical test, the Haar wavelets with $m_r = 3$ and 18 scaling functions are arranged on the boundary in figure 1. The DOF is $N = 18 \cdot 2^{m_r+1} = 288$. The time step width is $\Delta t = \beta \cdot \ell_{ref}/c$ ($\beta = 1$, $\ell_{ref} = 1/48$).

Figure 4 indicates the time history of the error $e(t)$ in the present method with truncation under several threshold parameters $\kappa$. If we prescribe the threshold parameter $\kappa$ into a value under a threshold, the error $e(t)$ is comparable to the one without truncation ($\kappa = 0$). The matrix compression with a larger value

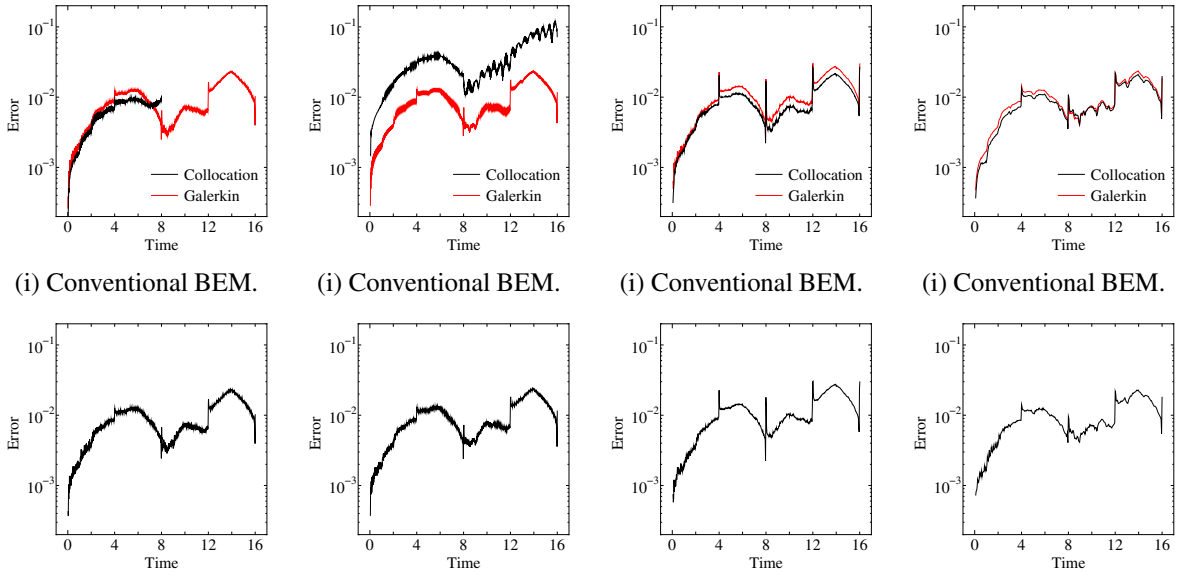


(i) Conventional BEM. (i) Conventional BEM. (i) Conventional BEM. (i) Conventional BEM.

(ii) Wavelet BEM. (ii) Wavelet BEM. (ii) Wavelet BEM. (ii) Wavelet BEM.

(a) $\beta = 0.3$. (b) $\beta = 0.5$. (c) $\beta = 0.7$. (d) $\beta = 1.0$.

**Figure 2.** The time history of the error $e(t)$ on the potential $u$ at the point A $(2, 25/48)$.

than the thresholding value leads to the rise of the error of the BE solutions because of the truncation error. We hence conclude that the truncation using a threshold $\kappa$ such as keeping the accuracy of the BE analysis results in the reduction of the memory requirement for the storage of the coefficient matrices.

We next show the compression rate of the coefficient matrix generated at an each time step in figure 5. The compression rate (%) is defined as

$$\text{Compression rate } (\%) := \frac{M_{store}}{N^2} \cdot 100, \tag{25}$$

where $N$ is the DOF, and $M_{store}$ is the number of stored entries of the coeffient matrix generated at the current time step. In the present BE analysis, the compression rate at the first time step indicates the one of the matrices in the left-hand side of Eq.(14). At the other time step, the results shown in figure 5 are the compression rates of the coefficient matrices for calculating the time convolution in the right hand side of Eq.(14).

In the early stage of the time marching, a number of the matrix entries have null values because of the causality condition of the fundamental solution for the time-domain boundary integral equation. The compression rates for the present wavelet method with every thresholding values are comparable to the one for the conventional piecewise constant BEM. The rise of the compression rates continues to the time when the scalar wave excited at the $t = 0$ approaches to the right side of the example domain. In the time range after this time, the number of the stored entries for the present wavelet method decreases with time, while the compression rate approaches to 100 % for the conventional BEM. The matrix compression by the present method is thus effective for the time-domain BE analysis in the long time range.

### *5.3. Reduction of computational work*

We finally discuss the reduction of the computational work by employing the present time-domain wavelet BEM. Figure 6 depicts the CPU time for generating the coefficient matrices, calculating the time convolution by matrix-vector multiplications and solving the discretized equations at every time step. In the present example, the most of the CPU time shown in figure 6 is spent on the generation of the coefficient matrix entries and the time convolution. The computation time for solving the discretized

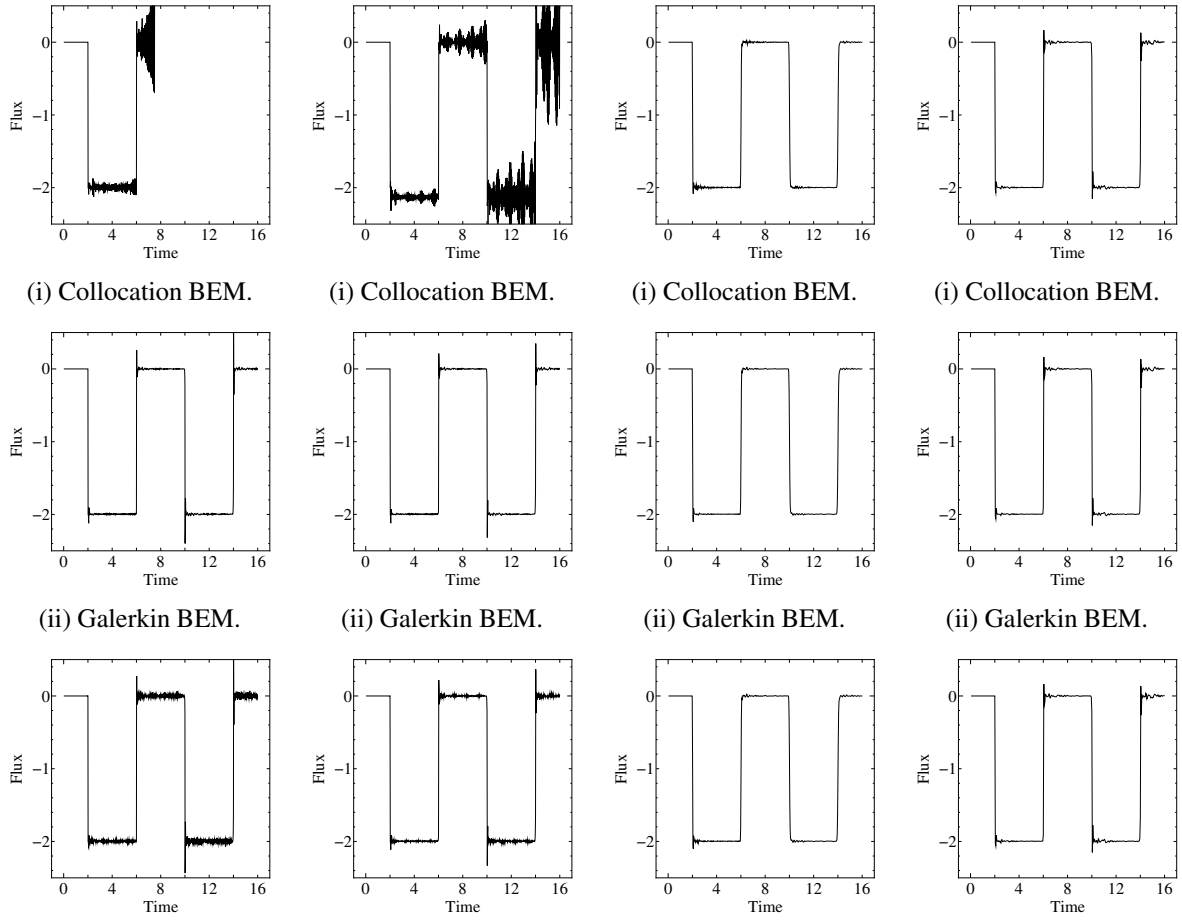


(i) Collocation BEM. (i) Collocation BEM. (i) Collocation BEM. (i) Collocation BEM.

(ii) Galerkin BEM. (ii) Galerkin BEM. (ii) Galerkin BEM. (ii) Galerkin BEM.

(iii) Wavelet BEM. (iii) Wavelet BEM. (iii) Wavelet BEM. (iii) Wavelet BEM.

(a) $\beta = 0.3$. (b) $\beta = 0.5$. (c) $\beta = 0.7$. (d) $\beta = 1.0$.

**Figure 3.** The time history of the flux $q$ at the point A $(2, 25/48)$.

equations using the GMRES is very short time because the system matrix of Eq.(14) is sparse for both the conventional- and the present wavelet BEM. The iterations of the GMRES is rapidly converged by the simple preconditioning like the Jacobi preconditioner, as shown in figure 7.

The time-domain wavelet BEM generates the sparse coefficient matrices by calculating the double boundary integrals divided into the sub-boundaries by the spline nodes (the points with the discontinuity of the Haar wavelets), which needs more computational work in the present wavelet BEM than the conventional BEM. The sparse matrix of the wavelet method results in the little computational work of the matrix-vector multiplication for the time convolution. The CPU time increasing with time in a early stage of the time-marching due to the causality condition turns to fall as the stored matrix entries are decreased. In the conventional time-domain BE analysis, the increase of the computational work with time is caused by the martix-vector multiplications because of little CPU time for generating the coefficient matrices. The CPU time at an each step for the wavelet BEM with truncation shortens finally than that for the conventional BEM; the total CPU time from the initial time step is greater than that of the conventional BEM. It is difficult to reduce the computational work of the time-domain BE analysis by the wavelet method, except for the cases that the wave propagation in a long time is simulated. This tendency on the computational work of the present method is different from the wavelet BEM for the Laplace problems and the Helmholtz problems.

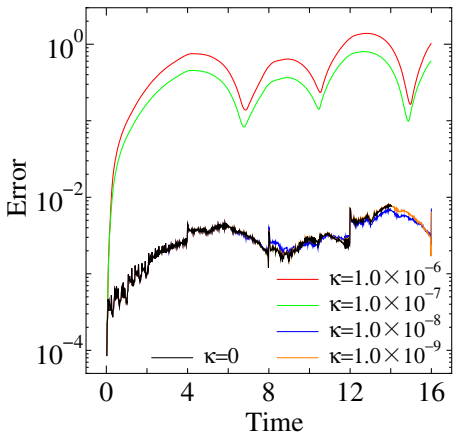


**Figure 4.** Time history of the error $e(t)$ ($N = 288$, $\beta = 1$, $\ell_{ref} = 1/48$).

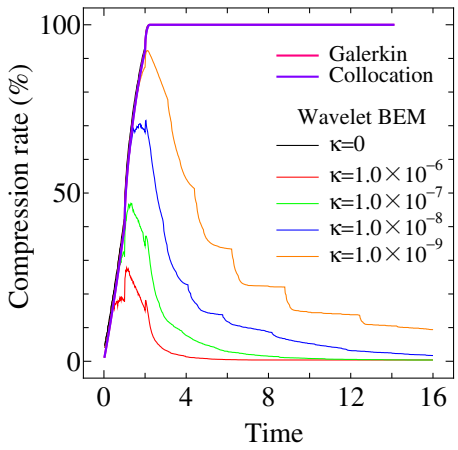


**Figure 5.** Compression rates of the coefficient matrices generated at each time step($N = 288$, $\beta = 1$, $\ell_{ref} = 1/48$).

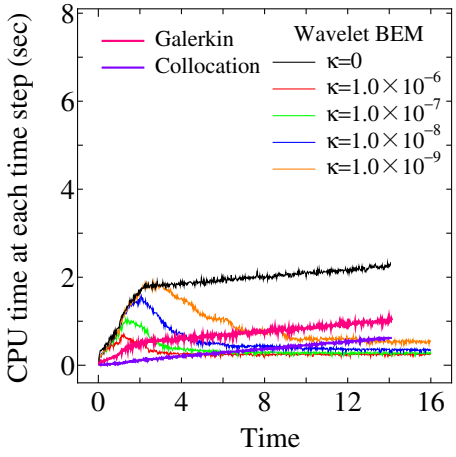


**Figure 6.** CPU time at each time step.

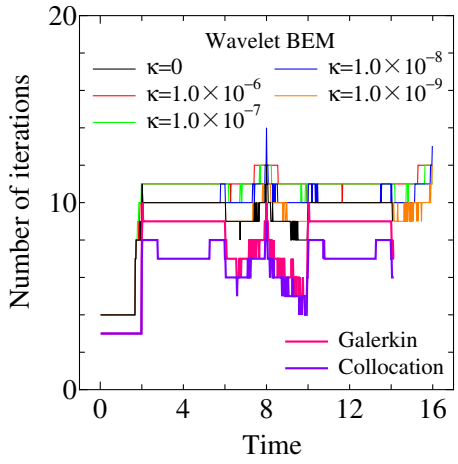


**Figure 7.** The number of iterations for solving the algebraic equation using the preconditioned GMRES at each time step.

## 6. Conclusions

We have developed the wavelet method for the time-domain BEM for 2-D scalar wave equation. The wavelet method has introduced to reduce the memory requirement and the computational work in this BE analysis. The performance of the present method has been investigated through the simulation results of a simple example. The present method has the numerical stability comparable to the conventional Galerkin BEM, while the BE solutions obtained by the conventional collocation BEM is unstable for a small time step like $\beta = c\Delta t/\ell_{ref} \leq 0.5$. The truncation of the small matrix entries enables us to reduce the memory requirement without the accuracy deterioration of the BE solution. The reduction of the computational work is difficult in the practical examples. This is because for the time-domain BEM (i) the most of the computational work is spent for generating the coefficient matrices and (ii) the CPU time for solving the algebraic equations with a sparse system is very short.

## References

[1] Nishimura N: Fast multipole accelerated boundary integral equation methods. 2002 *Appl. Mech. Rev.* **55**(4) 299–324
[2] Schneider R: Multiskalen- und Wavelet-Matrixkompression: Analysisbasierte Methoden zur effizienten Lösung großer vollbesetzter Gleichungssysteme. B.G.Teubner, Stuttgart, 1998.
[3] Koro K and Abe K Non-orthogonal spline wavelets for boundary element analysis 2001 *Engrg. Anals. Bound. Elems.* **25** 149-64
[4] Koro K and Abe K Wavelet Matrix-compression property of Beylkin-type truncation scheme for wavelet BEM 2003 *J. Appl. Mech. JSCE* **6** 301-10 (in Japanese)
[5] Beylkin G, Coifman R and Rokhlin V Fast wavelet transforms and numerical algorithms I 1991 *Comm. Pure Appl. Math.* **44** 144-83
[6] Koro K, Abe K and Tazaki H Application of discrete wavelet transform to wavelet collocation BEM 1999 *J. Appl. Mech. JSCE* **2** 153-62 (in Japanese)
[7] Bucher HF, Wrobel LC, Mansur WJ and Magluta C A novel approach to applying fast wavelet transforms in the boundary element method 2002 Electronic J. Bound. Elems. **BETEQ 2001**(2) 187-95
[8] Bucher HF, Wrobel LC, Mansur WJ and Magluta C On the block wavelet transform applied to the boundary element method 2004 *Engrg. Anals. Bound. Elems.* **28** 571-81
[9] Ravnik J, Škerget L and Hriberšek M The wavelet transform for BEM computational fluid dynamics 2004 *Engrg. Anals. Bound. Elems.* **28** 1303-14
[10] Ravnik J, Škerget L and Hriberšek M Two-dimensional velocity-vorticity based LES for the solution of natural convection in a differentially heated enclosure by wavelet transform based BEM and FEM 2006 *Engrg. Anals. Bound. Elems.* **30** 671-86
[11] Ravnik J, Škerget L, Hriberšek M and Žunič Z: Numerical simulation of dilute particle laden flows by wavelet BEM-FEM 2008 *Comput. Methods Appl. Mech. Engrg.* **197** 789-805
[12] Škerget L and Ravnik J BEM simulation of compressible fluid flow in an enclosure induced by thermoacoustic waves 2009 *Engrg. Anals. Bound. Elems.* **33** 561-71
[13] Mansur WJ and Brebbia CA Further development on the solution of the transient scalar wave equation. 1985 *Topics in Boundary Element Research*, ed. Brebbia CA (Springer-Verlag) 87-123
[14] Soares Jr. D and Mansur WJ An efficient time-truncated boundary element formulation applied to the solution of the two-dimensional scalar wave equation 2009 *Engrg. Anals. Bound. Elems.* **33** 43-53
[15] Soares Jr. D and Mansur WJ An efficient stabilized boundary element formulation for 2D time-domain acoustics and elastodynamics 2007 *Comput. Mech.* **40** 355-65
[16] Koro K, Igarashi K and Abe K: Computational efficiency of time-domain boundary integral equation method using wavelets for diffusion problems 2009 Trans. of JASCOME **9** 73-8 (in Japanese)
[17] Yu G, Mansur WJ, Carrer, JAM and Gong L Stability of Galerkin and collocation time domain boundary element methods as applied to the scalar wave equation 2000 *Comput. Struct.* **74** 495-506